C. R. Mecanique 340 (2012) 845–858

Contents lists available at SciVerse ScienceDirect

Comptes Rendus Mecanique

www.sciencedirect.com

Out of Equilibrium Dynamics

The "turbulent flame speed" of wrinkled premixed flames ☆

Moshe Matalon [a,*], Francesco Creta [b]

[a] University of Illinois at Urbana-Champaign, Urbana, IL 61801, USA
[b] University of Rome La Sapienza, 00185 Roma, Italy

ARTICLE INFO

Article history:
Available online 17 November 2012

Keywords:
Turbulent flame speed
Darrieus–Landau instability
Premixed flames
Wrinkled flames
Flamelets
Markstein length
Flame stretch

ABSTRACT

The determination of the *turbulent flame speed* is a central problem in combustion theory. Early studies by Damköhler and Shelkin resorted to geometrical and scaling arguments to deduce expressions for the turbulent flame speed and its dependence on turbulence intensity. A more rigorous approach was undertaken by Clavin and Williams who, based on a multi-scale asymptotic approach valid for weakly wrinkled flames, derived an expression that apart from a numerical factor recaptures the early result by Damköhler and Shelkin. The common denominator of the phenomenological and the more rigorous propositions is an increase in turbulent flame speed due solely to an increase in flame surface area. Various suggestions based on physical and/or experimental arguments have been also proposed, incorporating other functional parameters into the flame speed relation. The objective of this work is to extend the asymptotic results to a fully nonlinear regime that permits to systematically extract scaling laws for the turbulent flame speed that depend on turbulence intensity and scale, mixture composition and thermal expansion, flow conditions including effects of curvature and strain, and flame instabilities. To this end, we use a hybrid Navier–Stokes/front-capturing methodology, which consistently with the asymptotic model, treats the flame as a surface of density discontinuity separating burned and unburned gases. The present results are limited to positive Markstein length, corresponding to lean hydrocarbon–air or rich hydrogen–air mixtures, and to wrinkled flames of vanishingly small thickness, smaller that the smallest fluid scales. For simplicity we have considered here two-dimensional turbulence, which although lacks some features of real three-dimensional turbulence, is not detrimental when using the hydrodynamic model under consideration, because the turbulent flame retains its laminar structure and its interaction with turbulence is primarily advective/kinematic in nature.

1. Introduction

A fundamental problem in combustion theory, which has drawn much attention in the literature, is the determination of the *turbulent flame speed* identified as the mean propagation speed of a premixed flame in statistical steady state within a turbulent field, similar to the *laminar flame speed* defined as the propagation speed of a (planar and adiabatic) premixed flame into a quiescent mixture. However, unlike the latter, which is a unique thermochemical property of a given combustible mixture, the turbulent flame speed depends on the flow conditions and experimental configuration. Indeed, experimental data have exhibited a wide range of scatter [1] casting doubt on whether a well-defined flame speed may be identified. However, it has been observed that turbulent flames in tubes propagate a well-defined distance in a given time

☆ This article is dedicated to Paul Clavin for his distinctive contributions to flame theory, on the occasion of his 70th birthday.

* Corresponding author.
E-mail addresses: matalon@illinois.edu (M. Matalon), francesco.creta@uniroma1.it (F. Creta).

1631-0721/$ – see front matter
http://dx.doi.org/10.1016/j.crme.2012.10.031

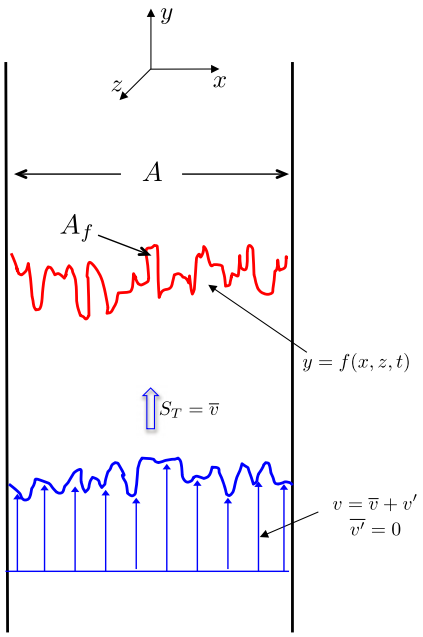

Fig. 1. Schematic representation of a wrinkled turbulent flame, illustrating the definition of the turbulent flame speed for a statistically stationary flame.

and Bunsen flames in statistically stationary turbulent flows possess a measurable average inclination angle, from which a representative flame speed can be identified. The practical importance of identifying a turbulent flame speed is evident allowing, for example, the determination of the mean fuel consumption rate in a combustor operating under turbulent conditions.

The turbulent flame speed can be properly defined if one resorts to the configuration shown in Fig. 1, where the flame described instantaneously by $y = f(x, z, t)$ is in statistical steady state within an isotropic homogeneous turbulent incident field. Decomposing the incident fluid velocity into a mean and fluctuating component, $\mathbf{v} = (u', \overline{v} + v', w')$, where an "overline" denotes the mean and primes denote the fluctuations, the transverse velocity components have zero mean due to homogeneity and the turbulent flame speed would be the mean longitudinal incoming velocity, i.e., $S_T = \overline{v}$. The mass flow rate through the entire flame is then given by $\dot{m} = \rho_u A S_T$, where ρ_u is the density of the fresh unburned gas. Since all the reactants pass through the wrinkled flame of area A_f, the mass flow rate can be equally calculated from the total contributions of mass flowing through all the differential segments comprising the wrinkled flame, assuming that each segment propagates normal to itself at the laminar flame speed S_L. Then $\dot{m} = \rho_u \overline{A_f} S_L$, which implies that $S_T/S_L = \overline{A_f}/A$. This relation was first noted by Damköhler [2] who resorted to geometrical arguments with analogy to a Bunsen flame to further deduce for large-scale turbulence that the area ratio could be approximated by $\overline{A_f}/A = 1 + v'_c/S_L$, where v'_c is the turbulent intensity (the r.m.s. of the velocity fluctuations), implying $S_T = v'_c + S_L$. Damköhler thus proposed for high-intensity turbulence ($v'_c \gg S_L$) the linear relation

$$\frac{S_T}{S_L} = \frac{v'_c}{S_L} \tag{1}$$

Shelkin [3] extended Damköhler's ideas arguing that as a result of the flame–vortex interaction, the wrinkled flame may be viewed as an ensemble of cones with bases proportional to the square of the turbulence integral scale ℓ and height proportional to v'_c multiplied by the representative eddy turnover time ℓ/S_L. He then deduced the relation $S_T/S_L = \sqrt{1 + (v'_c/S_L)^2}$, which reduces to Damköhler's result (1) for high-intensity turbulence ($v'_c \gg S_L$), and to the quadratic law

$$\frac{S_T}{S_L} = 1 + \frac{1}{2}\left(\frac{v'_c}{S_L}\right)^2 \tag{2}$$

for low intensity turbulence ($v'_c \ll S_L$).

Relying primarily on physical arguments, various studies attempted to reconcile the wide scatter in the experimental data proposing expressions of the form

$$\frac{S_T}{S_L} = 1 + C\left(\frac{v'_c}{S_L}\right)^n \tag{3}$$

with various constants C and adjustable exponents n (which include both Damköhler and Shelkin's formulas), or with explicit dependence on other functional parameters through dimensionless quantities including the Karlovitz number, the

Damköhler number and the turbulence Reynolds numbers; see the texts by Williams [4] and Peters [5] and the review articles by Bray [6], Lipatnikov and Chomiak [7] and Driscoll [8]. It is evident, however, that a single form on the basis of dimensional analysis cannot be justified and the expressions for the turbulent flame speed will vary in the different regimes of turbulence combustion.

A *rigorous approach* for the determination of the turbulent flame speed was initiated by Clavin and Williams [9] using a multi-scale perturbative analysis, further simplified by neglecting the effects of thermal expansion. They considered the ratio of laminar flame thickness to turbulent scale $\epsilon \ll 1$, thus treating the wrinkled flame as a perturbed planar flame, and the activation energy parameter large, confining chemical reactions to a thin reaction zone. Carrying the expansion to second order in ϵ, they derived the expression

$$S_T \sim S_L\left(1+\frac{1}{2}\overline{|\nabla f|^2}\right) \tag{4}$$

Since transverse gradients in their analysis are small, the flame sheet to leading order is simply advected by the local streamwise velocity fluctuations v', so that $\partial f/\partial t \sim v'$, where t represents time. Enforcing isotropy for the turbulence and a Taylor hypothesis for the fluctuating longitudinal displacement, they concluded that

$$\frac{S_T}{S_L} = 1+\left(\frac{v'_c}{S_L}\right)^2 \tag{5}$$

which differs from Shelkin's heuristic result (2) by the factor 1/2 in the second term and falls within the general expression (3). In subsequent work, Clavin and Williams [10] eliminated the hypothesis of negligible thermal expansion, but retained the assumptions of a weakly wrinkled flame, i.e., $f = O(\epsilon)$, and weak transverse velocities, i.e., $u', w' = O(\epsilon)$, implying that the flame up to this order is forced by the streamwise displacement of turbulence. This work reinstated their earlier result that the increase in speed of the turbulent flame is solely due to an area increase, and concluded that other effects that are likely to affect the turbulent flame speed, such as flame stretch and turbulence scale, would only arise at higher orders. A corrective term due to flame stretch was shown to arise when the analysis was taken to a higher order, but only after adopting the simplification of a constant density flow. A quadratic dependence of the turbulent flame speed on intensity was also recovered in a later study by Aldredge and Williams [11], highlighting in particular the influences of turbulence scale on the flame propagation.

The present work extends the aforementioned results by employing a similar but more general multi-scale approach that exploits the disparity between the distinct length scales associated with the fluid-dynamic field, the diffusion processes and the highly temperature-sensitive reaction rates. Viewed on the hydrodynamic scale the flame is a gasdynamic discontinuity separating burned from unburned gases, whose instantaneous shape and location is determined by the local flame speed obtained through asymptotic matching with the solution describing the diffusion and chemical reaction processes inside the flame zone [12]. The latter has been facilitated by the assumption that the activation energy of the chemical reactions is relatively large, implying that the chemistry is confined to a thin reactive–diffusive zone. The flame speed, defined as the propagation speed of the flame front relative to the unburned gas, is found to depend locally on both the curvature of the flame surface and the underlying hydrodynamic strain, which together constitute the total stretch rate experienced by the flame. Such dependence is modulated by a parameter on the order of the laminar flame thickness, known as the Markstein length, that measures the sensitivity to stretch and incorporates the effects of mixture composition and stoichiometry [13]. The resulting formulation is quite general, and consists of a nonlinear free-boundary hydrodynamic problem with jump conditions across the free surface – the flame – which, together with the flame speed relation, mimic the influences of the diffusion and chemical reaction processes occurring within the flame zone. The model is valid for realistic and $O(1)$ density variations, arbitrary and $O(1)$ flame displacements, and a general flow field whether laminar or turbulent. Most importantly, the formulation is free of modeling assumptions and ad-hoc parameters commonly used in turbulent studies. The clear advantage of the present asymptotic approach over Direct Numerical Simulation (DNS) is in the fact that the flame structure need not be fully resolved as it is ideally a surface of vanishing thickness for which the transport phenomena are accounted for through the general flame speed relation. Moreover, the flame location is uniquely and unambiguously determined eliminating the need to extract the information pertaining to the flame topology from the reacting flow field in an ad-hoc manner.

Due to its nonlinear nature, the hydrodynamic problem can no longer be treated analytically and is addressed here numerically using a hybrid Navier–Stokes/front capturing methodology, which was proven sufficiently robust and accurate [14–16]. The objective is formulating general scaling laws that include non-geometrical corrections to the turbulent flame speed, i.e., effects other than the increase in flame surface area exhibited in (5), with explicit dependence on: (i) turbulence parameters, such as intensity and scale, (ii) combustion parameters, such as mixture composition and thermal expansion, (iii) flow parameters, such as hydrodynamic strain, and (iv) combustion instability parameters associated with thermo-diffusive effects and the ubiquitous Darrieus–Landau (DL) instability resulting from the ever-present gas expansion. In this study we have focused on mixtures with positive Markstein length, corresponding to lean hydrocarbon–air or rich hydrogen–air mixtures, where diffusion effects have stabilizing influences and the hydrodynamic or DL instability is dominant. Thermo-diffusive instabilities arising in mixtures with negative Markstein length, corresponding to rich hydrocarbon–air or lean

hydrogen–air mixtures, would further contaminate the flame front with small-scale structures [17], adding nontrivial effects on the overall flame propagation that will be addressed in future work.

The flame, in the hydrodynamic model considered in this work, is assumed to retain its laminar structure, such that the only interaction with the turbulent field is advective/kinematic in nature. Such interactions are therefore precipitated by the energy-containing integral scales of turbulence, with the turbulent intensity v_c' representing the turnover velocity of eddies corresponding to such scales. Turbulent scales smaller than the laminar flame thickness and down to the Kolmogorov scale are, by definition, not energetic enough to distort or advect the flame and can therefore go under-resolved in the simulations. The present results are therefore strictly valid within the wrinkled-to-corrugated flamelet regimes of turbulent combustion [5]. Being limited to two-dimensions, the present simulations admittedly lack some features of real three-dimensional turbulence, such as vortex stretching. This, however, may not be detrimental because vortex stretching is a mechanism for the cascade of energy to smaller and smaller scales which, as pointed out earlier, need not be modeled in the present approach. Moreover, our objective is to extend the findings of the classical asymptotic theories, which do not account for such effects.

2. Formulation and numerical approach

In the hydrodynamic formulation, the flame is a gasdynamic discontinuity separating burned gas from the fresh unburned mixture, and may be described by the zero-level of the scalar function $\psi(\mathbf{x},t)$. The flow on either side of the flame front is governed by the Navier–Stokes equations

$$\nabla\cdot\mathbf{v}=0 \tag{6}$$

$$\rho\frac{\partial\mathbf{v}}{\partial t}+\rho(\mathbf{v}\cdot\nabla)\mathbf{v}=-\nabla p+\mu\nabla^2\mathbf{v} \tag{7}$$

where $\mathbf{v}$, p are the velocity and pressure fields, with the density given by

$$\rho=\begin{cases}\rho_u & \psi(\mathbf{x},t)<0\\ \rho_b & \psi(\mathbf{x},t)>0\end{cases} \tag{8}$$

The viscosity of the mixture μ could be equally expressed as a piecewise-constant function, but for simplicity it was assumed constant over the entire domain. Conservation of mass and momentum across the flame sheet is enforced through the Rankine–Hugoniot relations

$$\left[\!\left[\rho(\mathbf{v}\cdot\mathbf{n}-V_f)\right]\!\right]=0 \tag{9}$$

$$\left[\!\left[\mathbf{n}\times(\mathbf{v}\times\mathbf{n})\right]\!\right]=0 \tag{10}$$

$$\left[\!\left[p+\rho(\mathbf{v}\cdot\mathbf{n})(\mathbf{v}\cdot\mathbf{n}-V_f)\right]\!\right]=0 \tag{11}$$

where the operator $[\![\cdot]\!]$ defines the jump in the quantity across the flame sheet.

The unburned-to-burned density ratio, $\sigma=\rho_u/\rho_b$, or thermal expansion coefficient, is a measure of the heat released by the chemical reactions. Transport phenomena within the thin flame are accounted for through a general flame speed–flame stretch relation modulated by a Markstein length $\mathcal{L}$ that measures the sensitivity of the flame speed to geometric and flow nonuniformities. The flame speed is defined as the normal velocity of the unburnt gas relative to the flame front, namely $S_f=\mathbf{v}^*\cdot\mathbf{n}-V_f$, where $\mathbf{v}^*$ is the gas velocity evaluated at $\psi=0^-$, i.e., just ahead of the flame front, $V_f=-\psi_t/|\nabla\psi|$ is the propagation velocity in a laboratory fixed frame and $\mathbf{n}=\nabla\psi/|\nabla\psi|$ is the unit normal taken positive when pointing towards the burned gas ($\psi>0$). The flame speed–flame stretch relation takes the form

$$S_f=S_L-\mathcal{L}\mathbb{K} \tag{12}$$

where S_L is the laminar flame speed, and $\mathbb{K}=S_L\kappa+K_S$ is the flame stretch rate, which depends on the curvature $\kappa=-\nabla\cdot\mathbf{n}$ of the flame sheet, and the underlying hydrodynamic strain $K_S=-\mathbf{n}\cdot\mathbf{E}\cdot\mathbf{n}$, with $\mathbf{E}$ the rate of strain tensor. This relation could be also cast in the form of a level-set equation for the shape and location of the flame sheet,

$$\psi_t+\mathbf{v}^*\cdot\nabla\psi=S_f|\nabla\psi| \tag{13}$$

with S_f given by (12). The Markstein length

$$\mathcal{L}=\left\{\frac{\sigma\ln\sigma}{\sigma-1}+\frac{\beta(Le_{\text{eff}}-1)}{2(\sigma-1)}\int_1^\sigma\frac{\ln\xi}{\xi-1}\,\mathrm{d}\xi\right\}l_f \tag{14}$$

on the order of the laminar flame thickness l_f, mimics the influences of reaction and diffusion and thus depends on the mixture composition through the effective[1] Lewis number Le_{eff}, and its reactivity through the Zel'dovich or activation energy parameter (see [13] for additional details). In an experimental setting changes in $\mathcal{L}$ may be accommodated by varying the fuel type and mixture composition or the system pressure. For future reference, it is convenient to introduce the scaled Markstein number $\alpha = \mathcal{L}/L$. Conventionally the Markstein number is defined as the Markstein length scaled with respect to the laminar flame thickness, so that α here is in fact the product of the Markstein number and the relative flame thickness l_f/L.

The calculations reported below were carried out on a two-dimensional domain of transverse dimension L with periodic conditions imposed on both sides (see Figs. 4(a) and 5(a) below). Turbulence is introduced at the inflow by sweeping a pre-generated two-dimensional realization of incompressible, homogeneous, isotropic turbulence obtained as a solution of the Navier–Stokes equations with density ρ_u in a periodic domain. The longitudinal length was taken equal to 64 times the transverse length L, thus allowing a satisfactory statistical characterization. The incident turbulent field is characterized by an intensity v'_c, measured by the r.m.s. of the velocity fluctuations, and possesses well established autocorrelation properties defining the turbulence integral scale ℓ, as illustrated in Creta and Matalon [16].

To retain a continuum approach while solving the free-boundary hydrodynamic problem, the piecewise constant density across the flame is approximated by a *tanh*-like function over few grid cells and the Navier–Stokes equations modified by adding a source term for the divergence of the fluid velocity to account for the jump relation (9), as illustrated in [14,15]. The resulting equations were then solved on a uniform grid over the entire domain using a variable-density Navier–Stokes solver, ensuring that momentum conservation across the flame as expressed by the jump relations (10)–(11) is automatically satisfied. The flame dynamics was tracked via the level-set equation (13), and the resulting ψ-field was then used to approximate the density field (8). The determination of $\mathbf{v}^*$ on the Langragian mesh representing the flame surface, needed in the integration of (13), was realized using an immersed-boundary technique. The flame dynamics computations were carried out on a domain of longitudinal dimensions L to $2L$, as deemed necessary. The "numerical flame thickness" created by smearing the density jump was kept small, spanning as few as three-to-four grid points, while the smallest integral scales examined in this study were resolved with at least 12 grid points. In consistency with the asymptotic derivation, viscous effects, similar to other diffusion processes, constitute a higher order correction to flame propagation and were retained small during the calculations by adopting a relatively large Reynolds number $= 10^5$, while no claim is clearly made of resolving the corresponding turbulent field. No significant changes in the flame sheet behavior were detected when increasing the Reynolds number to 10^6.

The numerical methodology has been extensively validated in a number of recent publications: In a laminar setting, it reproduced analytical results of simple flame configurations [14], accurately described the initial flame growth of hydrodynamically unstable flames compared to the rigorous asymptotic linear stability results [12,18,19], and replicated the bifurcation characteristics of premixed flames known analytically from closed-form dispersion relations [15]. It has also accurately reproduced the analytical pole solutions of the Michelson–Sivashinsky (MS) equation that governs the nonlinear development of the Darrieus–Landau instability for weak thermal expansion [20]. In the turbulent regime it reproduced [16] most of the turbulent flame speed scaling laws obtained from a stochastic MS-type model [21].

3. Results

It is instructive to summarize first results concerning flame propagation into quiescent mixtures with $\mathcal{L} > 0$, i.e., corresponding to lean hydrocarbon–air or rich hydrogen–air mixtures, in a laminar setting. Under such conditions diffusion effects furnish stabilizing influences on short wavelength disturbances allowing the existence of *stable* planar flames [12,18,19]. Within the context of the hydrodynamic model (6)–(12) the exact dispersion relation shows that all disturbances of wavelength $\lambda < \lambda_c$, where $\lambda_c \equiv 2\pi[(3\sigma - 1)/\sigma - 1)]\mathcal{L}$, are damped [15] implying that planar flames are stable in domains of width $L < \lambda_c$. The critical transverse width λ_c depends of course on the mixture composition through $\mathcal{L}$, and on its reactivity through σ.

When the diffusive stabilizing effects are insufficient, i.e., $L > \lambda_c$ the planar flame becomes unstable and acquires a cusp-like conformation, a typical manifestation of the hydrodynamic, or Darrieus–Landau (DL) instability, caused by the gas expansion resulting from the significant temperature rise across the flame. These structures are stable[2] and propagate steadily at a constant speed U, substantially larger than the laminar flame speed. Fig. 2 shows two such flames corresponding to different values of $\alpha = 0.375$ and 0.019. We note that for a smaller value of the Markstein length the flame has a sharper peak and propagates faster. The figures clearly illustrate the deflection of streamlines across the flame that results from the large jump in the gas velocity component normal to the sheet associated with thermal expansion, and the vortical flow induced in the unburned gas (otherwise at rest), which is evidently responsible for the formation of the cusp-like flame structure.

[1] For a stoichiometric mixture the effective Lewis number is the average of the individual Lewis numbers of the fuel and oxidizers; for an off-stoichiometric mixture the deficient component is more heavily weighted to the extent that for sufficiently lean mixtures it is practically the Lewis number of the fuel and for sufficiently rich mixtures it is the Lewis number of the oxidizer.

[2] The stability of the cusp-like structures was only proved for $\sigma - 1 \ll 1$, in which case they are obtained as exact analytic solutions of the MS equation, also known as pole solutions [22,23]. For $\sigma - 1 = O(1)$, this conclusion was established numerically [15,20].

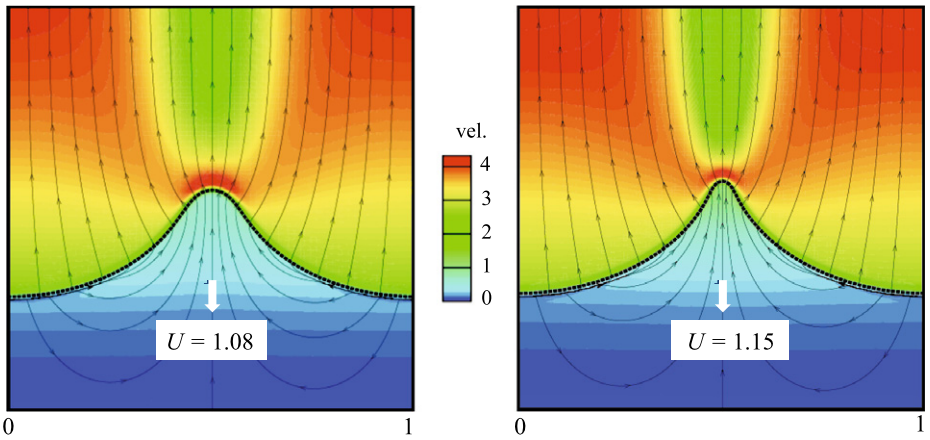

Fig. 2. Streamline pattern across steadily propagating (downwards) cusp-like hydrodynamically unstable flames, calculated for $\sigma = 4$ and corresponding to $\alpha = 0.375$ (left figure) and $\alpha = 0.019$ (right figure). The propagation velocity U and the magnitude of the gas velocity (see legend) are scaled with respect to S_L.

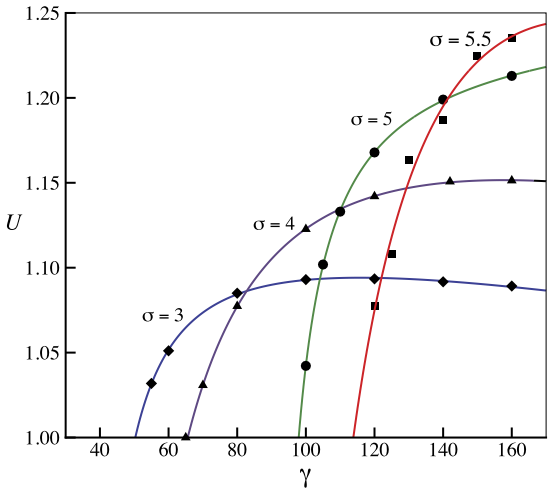

Fig. 3. Bifurcation diagram, showing the dependence of the flame propagating speed (in units of S_L) on the parameter $\gamma \equiv (\sigma - 1)/\alpha$ for various values of σ.

Fig. 3 shows the dependence of the speed U, in units of S_L, of steadily-propagating flames on the parameter $\gamma \equiv (\sigma - 1)/\alpha$ for several values of σ. The intersection of each curve with the abscissa identifies the corresponding bifurcation point[3] $\gamma_c = 2\pi(3\sigma - 1)$ beyond which the planar flame loses stability to a cusp-like conformation that propagates at a speed U larger than the laminar flame speed S_L. As σ increases the bifurcation is delayed to larger value of γ and the evolving structure propagates at a significantly larger speed, an increase of 20–25% for realistic values of σ ranging between 5 and 6. In terms of the Markstein number α, the bifurcation occurs at $\alpha_c = (\sigma - 1)/2\pi(3\sigma - 1)$, with sub-critical planar flames observed for $\alpha > \alpha_c$ and supercritical corrugated flames observed for $\alpha < \alpha_c$.

While the effect of the DL instability is well understood in the laminar setting, its role within the more complex turbulent combustion regime remains to be clarified. Numerical simulations of premixed flames subjected to weak velocity fluctuations [24] or propagating through vortex arrays that mimic the effect of turbulence [25], have attributed the wrinkling of the flame surface and the accompanied increase in speed to the DL instability. Few numerical studies [26,27] were devoted directly to this phenomenon, concluding that its influence on turbulent flames is limited to low turbulent intensities. More general conclusions, however, are extremely difficult to extract from numerical simulations as the bifurcative properties of the flame could not be clearly outlined. Experimental evidence [28–34], on the other hand, suggests that the DL instability can definitely play an important role in turbulent flame propagation. The present work provides a systematic investigation of this phenomenon based on physical first principles.

[3] With strain neglected, i.e., the local flame speed depending only on curvature, the bifurcation point is found to be at a slightly lower value $\gamma_c = 4\pi\sigma$.

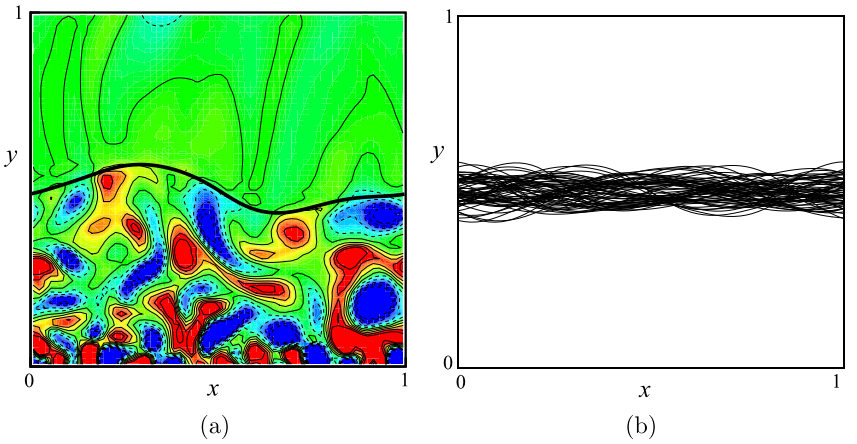

Fig. 4. Statistically stationary turbulent flames (shown as solid dark curves) for sub-critical conditions corresponding to $\alpha = 0.078$. (a) The turbulent flow field; vorticity contours are identified with (red/blue) solid/dashed lines for positive/negative values. (b) The flame brush; instantaneous flame profiles are plotted at consecutive time intervals. The incident turbulent field is characterized by a turbulence intensity $v'_c = 0.4$ and scale $\ell = 0.1$, and the combustion field by $\sigma = 5$. Length are measured in units of L and speed in units of S_L.

The quiescent setting used under laminar conditions is now replaced by a pre-generated two-dimensional realization of homogeneous isotropic turbulence fed as an inflow at a constant speed, as discussed above. The resulting incident turbulent flow field $(u', \overline{v} + v')$ is characterized by an intensity v'_c and integral scale ℓ. The flame was kept statistically stationary at a specified location by adjusting the mean inflow velocity in a closed loop control system, as shown in [21]. The control system was implemented on the turbulent intensity as well, keeping v'_c just ahead of the flame at a given user-specified value. The turbulent flame speed is, by definition, equal to the constant average inflow velocity, i.e., $S_T = \overline{v}$. Let the flame surface be expressed in the form $\psi(x, y, t) \equiv y - f(x, t)$, the level set equation (13) becomes

$$\overline{v} + v' - u' f_x - f_t = S_f \sqrt{1 + f_x^2}$$

where subscripts denote partial differentiation. Averaging in transverse direction x and in time, noting that $\overline{u' f_x} = 0$, yields an expression for the turbulent flame speed

$$S_T = \overline{S_f \sqrt{1 + f_x^2}} \tag{15}$$

If one assumes that the local flame speed is everywhere equal to the constant laminar flame speed S_L, the relation

$$\frac{S_T}{S_L} = \overline{\sqrt{1 + f_x^2}} \tag{16}$$

is obtained, which is consistent with Damköhler's observation that the increase in speed of the turbulent flame is due to the increased surface area of the flame front. This expression also simplifies to Eq. (5) derived by Clavin and Williams by bringing the average inside the square root and assuming that transverse gradients are small ($f_x \ll 1$). The more general expression (12) considered here for the local flame speed suggests that there may be contributions other than area increase to the turbulent flame speed.

Results show significant different flame conformations for sub- and super-critical conditions, where criticality corresponds to the well-defined conditions associated with the laminar setting. For sub-critical conditions the flame remains planar on the average, as shown in Fig. 4, with its mean location retained at $y = 0.5$. The solid dark curve in Fig. 4(a) is the flame surface; the solid/dashed (red/blue) contours represent clockwise/counterclockwise vorticity isocurves and illustrate the turbulent nature of the flow field. Average vorticity downstream of the flame is reduced due to the effect of volumetric expansion. The instantaneous flame profiles shown in Fig. 4(b) at equal and consecutive time intervals demonstrate that the flame brush remains statistically planar.

For super-critical conditions the flame surface is highly corrugated, as shown in Fig. 5, resembling the cusp-like conformations of the laminar case that are consequences of the DL instability. The mean location of the flame remains at $y = 0.5$ and the longer computational domain is necessary to capture instances when the flame front reaches distances close to and beyond $y = 1$. Sharper cusps introduce more pronounced velocity gradients acting as sources of vorticity, contrasting the volumetric expansion effect. The instantaneous flame profiles shown in Fig. 5(b) at equal and consecutive time intervals attest for the much wider flame brush with sharp intrusions into the burned gas.

The difference between the two cases is striking in many respects. Firstly, the sub-critical case possesses an intrinsic statistical symmetry which appears evident upon computation of probability density functions (pdf) for the instantaneous flame location f and local curvature κ, as shown in Fig. 6. The increase in variance with turbulent intensity indicates

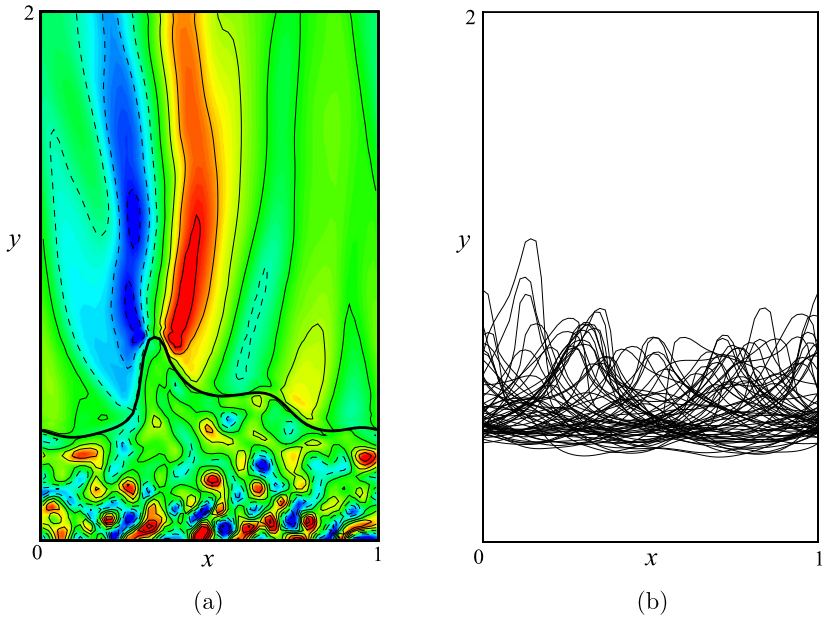

Fig. 5. Statistically stationary turbulent flames (shown as solid dark curves) for supercritical conditions corresponding to $\alpha = 0.017$. (a) The turbulent flow field; vorticity contours are identified with (red/blue) solid/dashed lines for positive/negative values. (b) The flame brush; instantaneous flame profiles are plotted at consecutive time intervals. The incident turbulent field is characterized by a turbulence intensity $v'_c = 0.4$ and scale $\ell = 0.1$, and the combustion field by $\sigma = 5$. Length are measured in units of L and speed in units of S_L.

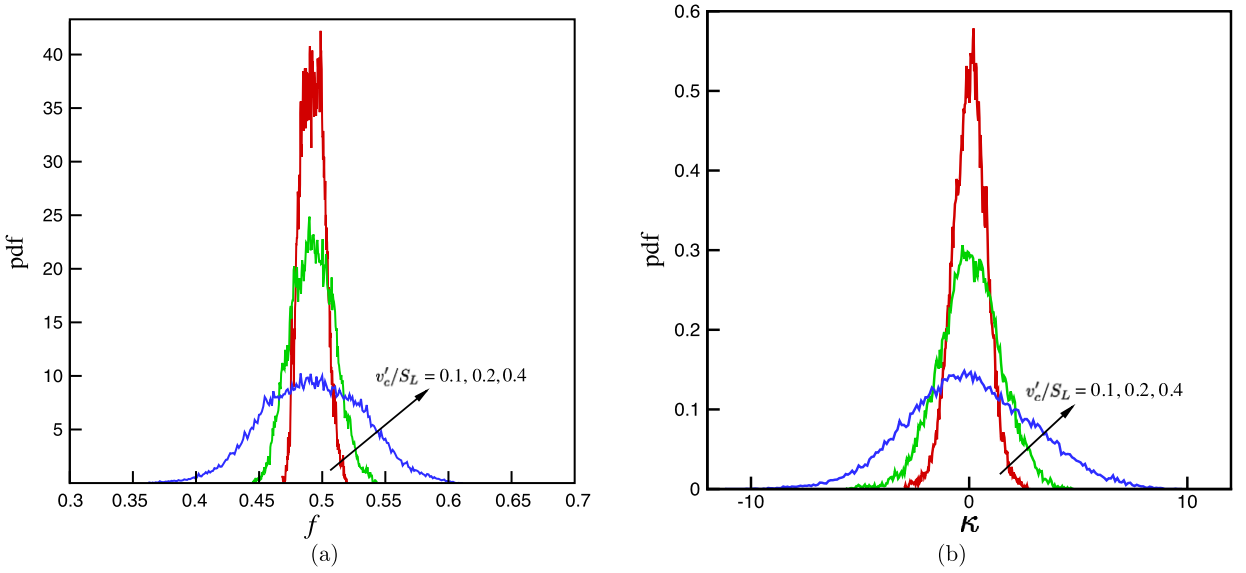

Fig. 6. Probability density functions of (a) flame position and (b) flame surface curvature for sub-critical conditions, parametrized with the turbulence intensity v'_c/S_L. Calculated for $\sigma = 5$ and $\alpha = 0.066$.

thicker flame brushes and higher local curvatures. The mean curvature, however, remains zero, confirming that the overall structure remains planar with equally probable convex and concave conformations. Further examination reveals that thermal expansion does not have an effect on flame curvature at any given turbulent intensity. This result is consistent with the experimental data presented in [29] showing pdf's of flame curvature for methane and propane. Despite the significantly higher heat of combustion of propane, the pdf's of both fuels are close to each other to within experimental error. Thermal expansion, on the other hand, has a substantial influence on the flame displacement pdf and consequently on the brush thickness, as illustrated in Fig. 7(a). The pdf's shown in this figure for the three values $\sigma = 4, 5, 6$, which may correspond to methane/ethane/propane flames having increasingly larger heat release in proportion $1 : 1.8 : 2.6$, imply that wider brushes result for more energetic fuels. This dependence has an immediate consequence on the overall flame surface area and the flame propagation speed as discussed below. In Fig. 7(b) the probability density function of the flame curvature is shown for

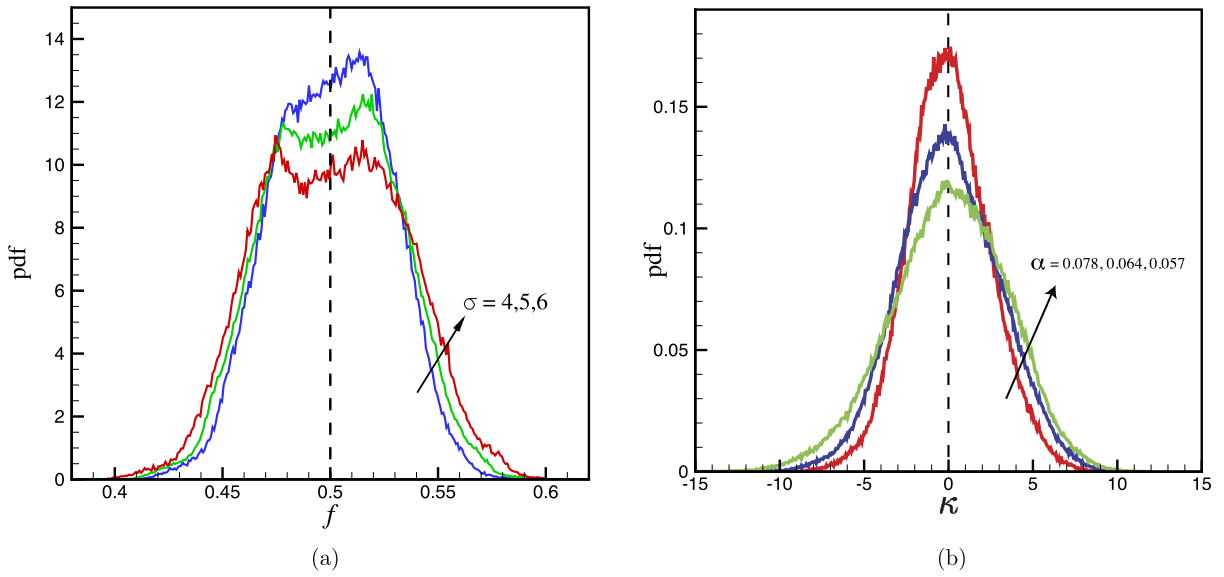

Fig. 7. Probability density functions of (a) flame location, parametrized with the thermal expansion parameter σ for a sub-critical flame with $\alpha = 0.078$, and (b) flame curvature, parametrized with the scaled Markstein number α for sub-critical conditions; calculated for $v'_c/S_L = 0.4$ and $\sigma = 5$.

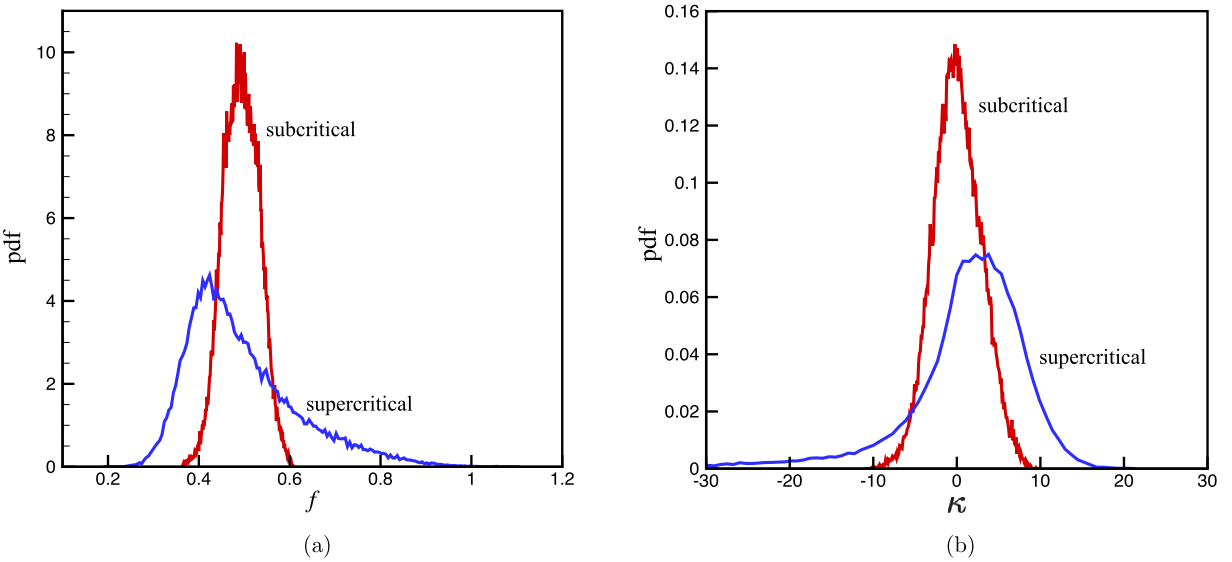

Fig. 8. Comparison of the probability density functions for flame position and curvature for (a) sub-critical ($\alpha = 0.066$) and (b) supercritical ($\alpha = 0.022$) conditions. Calculated for $v'_c/S_L = 0.4$ and $\sigma = 5$.

different values of the Markstein number α. The variance of these distributions increases as α decreases indicating higher local curvatures, which is a clear manifestation of the DL instability in terms of the proximity to the bifurcation point. Similar pdf's plotted for the flame displacement for various values of α show correspondingly thicker flame brushes. Thus, contrary to the laminar behavior where the flame for sub-critical conditions is stable, in a turbulent setting it is continuously influenced by the DL instability phenomenon in a range of α extending sufficiently away from the bifurcation point. We note that a decrease in $\mathcal{L}$, which is proportional to the laminar flame thickness, may be brought about by an increase in pressure. Our results, therefore, have the identical trend shown in the experimental pdf's reported in [35] for methane–air flames, where an intensification in flame curvature was detected by increasing the pressure. It should be noted that given the different experimental setup and operating conditions reported in the literature, which require a crude estimate of the various parameters, a direct comparison with the theoretical predictions is fortuitous.

The symmetry of the probability density functions that characterize sub-critical flames disappears for supercritical conditions and both, displacement and curvature pdf's are skewed towards the unburned side, as shown in Fig. 8. The asymmetry in the statistical data highlights the cusp-like shape of the flame, rounded towards the unburned side and sharp towards the

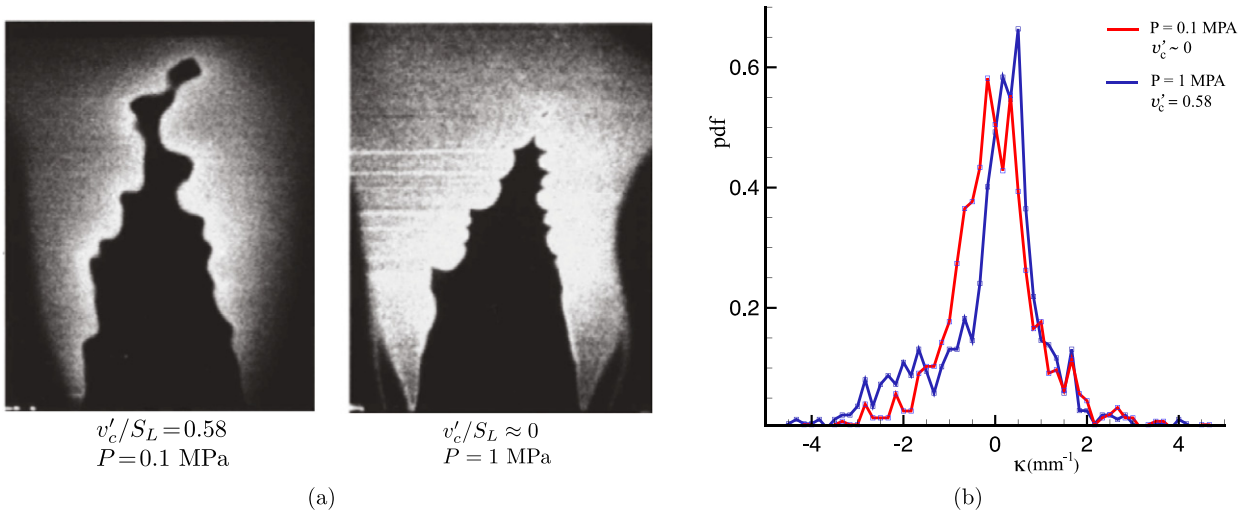

Fig. 9. (a) Images of turbulent Bunsen CH_4/air flames at various pressure and turbulent conditions; taken from [33]. (b) Probability density function of the flame curvature obtained from the scanned experimental images.

burned side, and is a direct consequence of the Darrieus–Landau instability. The pdf's displayed in Fig. 9(b) and extracted using a front recognition technique by Troiani [36] from scanned figures of flames taken from Kobayashi and Kawazoe's experiments [33] have a remarkably similar shape to the theoretical predictions. Fig. 9(a) shows the images of two such flames obtained under various pressure conditions. Since the bifurcation parameter γ is inversely proportional to the Markstein length, itself proportional to the laminar flame thickness, the parameter γ increases with increasing pressure. Consequently, the flame at 0.1 MPa corresponds to sub-critical conditions and that at 1 MPa to super-critical conditions. Indeed, similar to our theoretical predictions, the pdf for sub-critical flames is nearly symmetric, and for supercritical conditions it exhibits an asymmetry with the flame attaining large negative curvature values and more frequent small positive values.

We note that, unlike the laminar case, the "bifurcation" phenomenon in the turbulent regime occurs over a transition region, where the statistical symmetry that characterizes the pdf's for the flame location and curvature in the sub-critical regime gradually disappears. The transitional changes in the flame behavior and its statistical properties were discussed in [37].

The differences in flame behavior for sub- and super-critical conditions prompt different scaling laws for the turbulent flame speed, which are discussed next.

Starting with the sub-critical case, we first neglect the effect of strain by setting $K_S = 0$ in the flame speed relation (12). Since the mean curvature $\bar{\kappa} = 0$, the flame experiences no net stretch and the relation (3) reduces to (16) where the sole contribution to the turbulent flame speed is the area increase due to wrinkling. Under such conditions the turbulent flame speed follows a quadratic scaling law with respect to the turbulence intensity, as shown in Fig. 10, consistent with the early propositions [2,3,9,10]. The figure displays the propagation speed along with quadratic fits for several values of σ, including the independent result for $\sigma - 1 \ll 1$ that were obtained from the weakly nonlinear stochastic MS equation suitably modified to accommodate for a noise term mimicking turbulence [21]. What distinguishes the present result from the early predictions is the explicit dependence of S_T on thermal expansion σ, turbulence integral scale ℓ, and Markstein number α, which may be cast [21,37] in the form

$$\frac{S_T}{S_L} = 1 + \frac{b(\ell,\alpha)\, c(\sigma)}{\mathcal{L}/L}\left(\frac{v'_c}{S_L}\right)^2 \tag{17}$$

For a specified ℓ, the reciprocal of the Markstein number $1/\alpha$, acting effectively as the instability parameter, yields a substantial progressive linear increase in the turbulent flame speed S_T over the laminar value, as shown in Fig. 11(a). The slight departure from the linear curve at $\alpha^{-1} \approx 18$ for the case corresponding to $v'_c/S_L = 0.4$ is due to its proximity to the bifurcation point, which for $\sigma = 5$ occurs at $\alpha_c^{-1} = 15.7$. Hence, the turbulent flame speed is continuously affected by the DL instability in a regime where, in the absence of turbulence, the flame will be absolutely stable. The coefficient $b(\ell,\alpha)$ accounts for the dependence of the turbulent flame speed on the integral scale, shown in Fig. 11(b). The results reveals the existence of an intermediate scale $\ell^*/L \approx 0.62$, which remains nearly constant, that maximizes S_T. Eddies of this size are therefore most effective in disturbing the flame front, while smaller eddies become less and less effective. The amplification of the turbulent flame speed at ℓ^* is more modest as α decreases, namely upon approaching the bifurcation point. Note that for $\sigma = 4$, the critical Markstein number $\alpha_c = 0.06$. The dependence on thermal expansion through $c(\sigma)$ highlights the fact that an increase in heat release enhances the turbulent flame speed, an effect that levels off at sufficiently large values of σ. For given ℓ the coefficient c appears independent of the turbulent intensity and of the influence of the DL instability, as shown in [37]. Finally, we note that a similar dependence of S_T on the various parameters was obtained via the forced

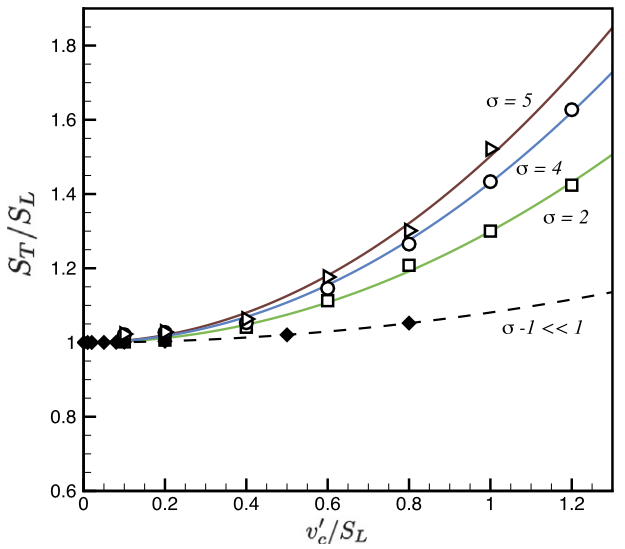

Fig. 10. The dependence of the turbulent flame speed, in the absence of hydrodynamic strain, on turbulence intensity, parametrized with the thermal expansion parameter σ and calculated for $\ell = 0.1$ and $\alpha = 0.066$. The symbols correspond to the calculated values and the solid line the quadratic fit.

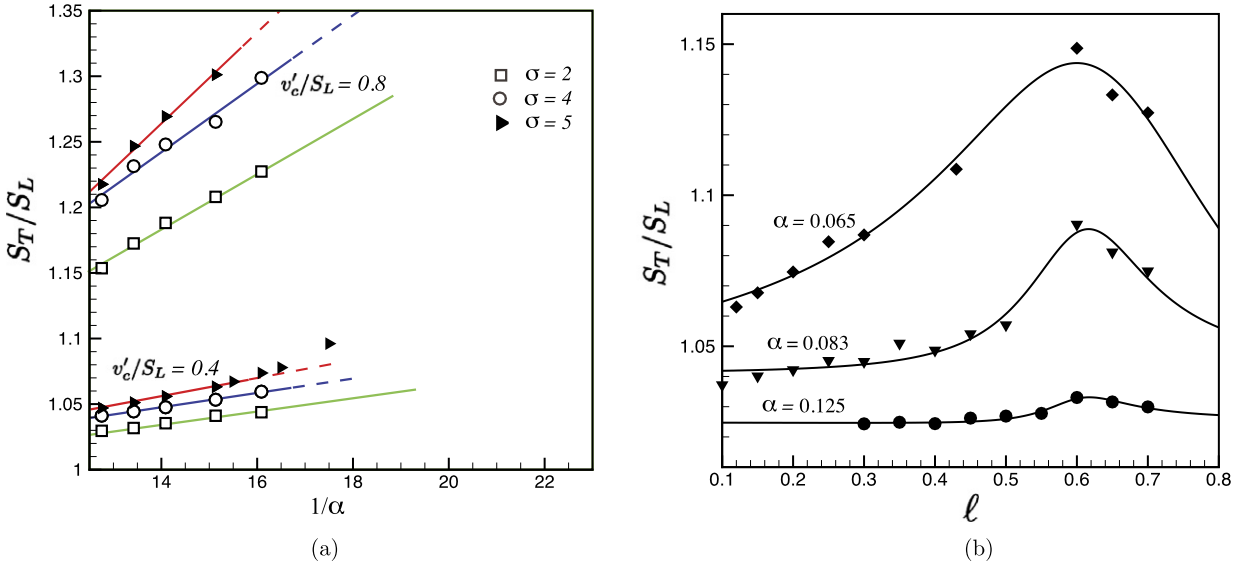

Fig. 11. The dependence of the turbulent flame speed, in the absence of hydrodynamic strain, on (a) the instability parameter $1/\alpha$, parametrized with the thermal expansion parameter σ, for two values of v'_c and $\ell/L = 0.1$, and on (b) the turbulence integral scale (in units of L), parametrized with the Markstein number α, for $\sigma = 4$ and $v'_c/S_L = 0.4$. In both cases, the symbols correspond to the calculated values and the solid curves to the linear or best fit, respectively.

MS model [15], which is valid for weak thermal expansion ($\sigma - 1 \ll 1$), providing further validation to the proposed scaling law.

We now incorporate the effect of hydrodynamic strain K_S in the flame speed relation (12), thus accounting for the complete effects of stretch. The statistical flame properties during turbulent propagation under sub-critical conditions reveal that, although the mean curvature is zero, the mean hydrodynamic strain is positive, i.e., $\overline{K_S} > 0$. The turbulent flame is therefore positively stretched and, for the positive Markstein length considered here, the mean flame speed $\overline{S_f} = S_L - \mathcal{L}\overline{K_S}$ decreases with increasing turbulence intensity. This tendency is a direct consequence of the imbalance between the thermal and mass diffusivities that characterize mixtures with a Lewis number sufficiently larger than one, or $\mathcal{L} > 0$. The flame under such circumstances tends to lose heat at a greater rate than the fuel is replenished by diffusion, and therefore propagates at a slower speed. This effect leads to a decrease in the turbulent flame speed S_T, at least for moderate intensities, until the increase in flame surface area counterbalances the effect of stretch and dominates the propagation. When rescaling

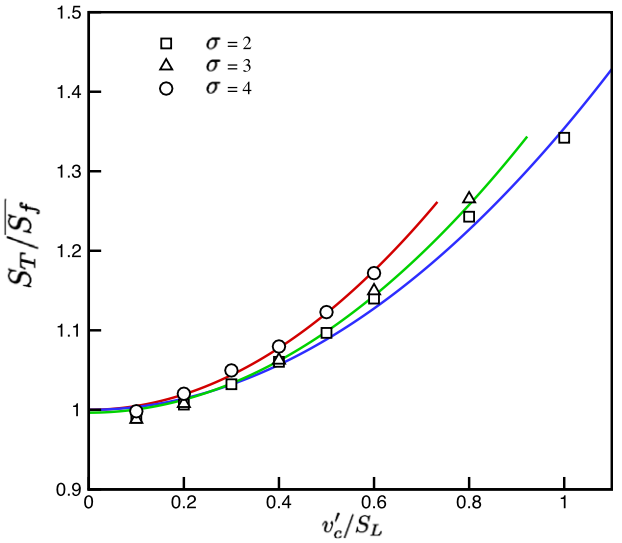

Fig. 12. The dependence of the turbulent flame speed scaled with the mean propagation speed, with hydrodynamic strain included, on turbulence intensity, parametrized with thermal expansion σ, and calculated for $\ell = 0.1$ and $\alpha = 0.066$. The symbols represent calculated values and the solid line the quadratic fit.

the turbulent flame speed with the mean flame speed $\overline{S_f}$, one recovers the quadratic dependence of S_T on intensity, as shown in Fig. 12. This suggests a modification to the previously proposed scaling law (17), in the form

$$\frac{S_T}{S_L} = \left[1 - \frac{\mathcal{L}\overline{K_S}}{S_L}\right]\left[1 + \frac{\hat{b}(\ell,\alpha)\,\hat{c}(\sigma)}{\mathcal{L}/L}\left(\frac{v'_c}{S_L}\right)^2\right] \tag{18}$$

which is found to retain the same dependence on v'_c and on the Markstein length [37], but must accommodate slight modifications in the dependence on σ and ℓ. The dependence on thermal expansion is not expected to conform with the strain-free dependence $c(\sigma)$, because flame area increase affected by thermal expansion becomes more enhanced in the present circumstances only at higher turbulence intensities. These adjustments remain to be determined. Finally we note that no counterpart results could be extracted from the stochastic MS equation because the weakly disturbed flow resulting with the weak thermal expansion assumption excludes strain rate effects.

In the supercritical regime the turbulent flame speed has a more complex dependence on the functional parameters, which has not been fully investigated. Preliminary results, with strain effects neglected, suggest that the turbulent flame speed conforms to an expression of the form

$$\frac{S_T}{S_L} = 1 + \frac{\tilde{b}(\ell,\alpha)\tilde{c}(\sigma)}{(\mathcal{L}/L)^m}\left(\frac{v'_c}{S_L}\right)^n \tag{19}$$

with exponents n and m that depend, in general, on the turbulence intensity and the thermal expansion parameter. The dependence of S_T on turbulence intensity shown in Fig. 13 clearly identifies different behaviors. In the low intensity regime the exponent n is less than one and varies between 0.68 and 0.88 depending on σ. This highlights the interesting observation that the cusp-like structures resulting from the DL instability are less sensitive to turbulence than planar flames. In the moderate intensity regime the exponent n is larger than one, and reaches the value 2 only for sufficiently large values of σ. Thus, despite their resilience to turbulence, the flames acquire more frequently elongated structures pointing towards the burned gas that result in increased flame surface area and thicker flame brush (see Fig. 5). As a result the turbulent propagation speed increases dramatically ($\tilde{b}\tilde{c} > bc$) and for moderate intensities could exceed the laminar flame speed significantly (see Fig. 13). The dependence of S_T on the instability parameter α^{-1} was found to be less than the linear dependence of sub-critical flames, i.e., with an exponent $m < 1$. The dependence of S_T on the integral scale, through $\tilde{b}$, confirms here too the existence of a scale that maximizes the turbulent flame speed [21]. However, the maximizing integral scale ℓ^* is lower than the corresponding scale for planar flames (sub-critical conditions), suggesting that as the flame becomes highly corrugated, smaller eddies become more and more effective in disturbing the flame front.

These results are corroborated by the stochastic MS model where it was clearly established that for $\sigma - 1 \ll 1$ the exponents take values $n < 2$ and $m < 1$ that depend on the turbulence intensity [15]. They are also consistent with the experimental observations of Kobayashi and co-workers [28,30,38] who proposed a relation for the turbulent propagation speed of the form $S_T/S_L \sim (P/P_0)^m (v'_c/S_L)^n$ to correlate their experimental observations of methane and propane turbulent flames, and deduced for the specified operating conditions the values $n \approx m \approx 0.4$ for the exponents. As noted earlier the effect of pressure is analogous to the effect of α^{-1}, which identifies the parallel between Kobayashi's proposition and the correlation (19).

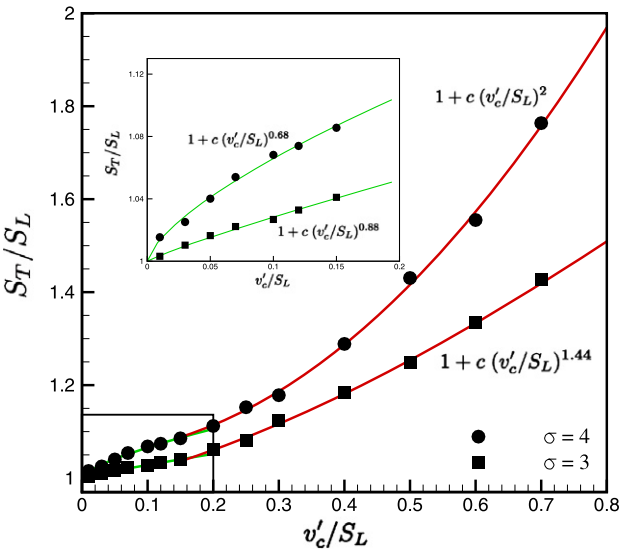

Fig. 13. The dependence of the turbulent flame speed, in the absence of hydrodynamic strain, on turbulence intensity, parametrized with thermal expansion σ, and calculated for $\ell = 0.1$ and $\alpha = 0.0167$. The symbols correspond to the calculated values and the solid lines a fit to the indicated expressions.

It must be emphasized that our predictions in the supercritical regime do not account for hydrodynamic strain, which could have a more prominent effect on the turbulent propagation of the corrugated flames resulting from the DL instability than the nearly-planar flames in the sub-critical regime, because of the overall stretch caused by the intense velocities ahead of the highly curved flames induced by thermal expansion. Moreover, the adopted explicit form of the flame surface, $y = f(x,t)$, prevents the flame to attain folded conformations, limiting the results to relatively low intensities. These effects are likely to have an important effect in the moderate-to-high intensity regime and could possibly be responsible for the so-called "bending effect", whereby the dependence of the turbulent flame speed on intensity levels off for $v'_c/S_L \gg 1$.

4. Conclusions

The present results extend the asymptotic perturbative approach initiated by Clavin and Williams [9,10] for the determination of the turbulent flame speed to a fully nonlinear regime via a hybrid front-tracking/Navier–Stokes methodology. The approach, which is based on physical first principles, is free of modeling assumptions and ad-hoc parameters, but is limited to the wrinkled-to-corrugated flamelet regime of turbulent combustion where the thin flame is not disturbed by the turbulence and retains its laminar structure. Attention has been restricted to mixtures corresponding to positive Markstein length, excluding thermo-diffusive instabilities that may further contaminate the flame surface with small-scale structures. The results identify and quantify various functional parameters, other than flame surface area increase, that affect the turbulent propagation. Different scaling laws are proposed for sub-critical conditions, where the flame remains statistically planar, and supercritical conditions, where the flame is highly corrugated with increasingly sharp crests pointing towards the burned gas. The different structures of the turbulent flame brush observed in these regimes are confirmed by their distinct statistical distributions. The proposed correlations obtained here would be more difficult to obtain from fully resolved DNS, not only because of the high resolution required in such computations, but also because of the ad-hoc identification of contours representing the flame surface from which to extract the necessary information, a choice that may not be uniquely identified.

Acknowledgements

This work has been partially supported by the National Science Foundation under Grant CBET-1067259. The authors are indebted to Navin Fogla who have helped in preparing some of the figures presented in this article.

References

[1] D. Bradley, How fast can we burn, Proceedings of the Combustion Institute 24 (1992) 247–262.
[2] G. Damköhler, Der Einfluss der Turbulenz auf die Flammengeschwindigkeit in Gasgemischen, Zeitschrift Für Elektrochemie 46 (1940) 601–652.
[3] K.I. Shelkin, On combustion in a turbulent flow, NACA TM 1110 (1947).
[4] F.A. Williams, Combustion Theory, 2nd edition, Benjamin/Cummings, Menlo Park, 1985.
[5] N. Peters, Turbulent Combustion, Cambridge University Press, 2000.
[6] K.N.C. Bray, Studies of the turbulent burning velocity, Proceedings of the Royal Society A: Mathematical and Physical Sciences 431 (1990) 315–335.
[7] A.N. Lipatnikov, J. Chomiak, Turbulent flame speed and thickness: Phenomenology evaluation and application in multi-dimensional simulations, Progress in Energy and Combustion Science 28 (2002) 1–74.

[8] J.F. Driscoll, Turbulent premixed combustion: Flamelet structure and its effect on turbulent burning velocities, Progress in Energy and Combustion Science 34 (1) (2008) 91–134.
[9] P. Clavin, F.A. Williams, Theory of premixed flame propagation in large-scale turbulence, Journal of Fluid Mechanics 90 (1979) 589–604.
[10] P. Clavin, F.A. Williams, Effects of molecular diffusion and thermal expansion on the structure and dynamics of premixed flames in turbulent flows of large scales and low intensity, Journal of Fluid Mechanics 116 (1982) 251.
[11] R.C. Aldredge, F.A. Williams, Influence of wrinkled premixed-flame dynamics on large-scale, low intensity turbulent flow, Journal of Fluid Mechanics 228 (1991) 487–511.
[12] M. Matalon, B.J. Matkowsky, Flames as gasdynamic discontinuities, Journal of Fluid Mechanics 124 (1982) 239–259.
[13] M. Matalon, C. Cui, J.K. Bechtold, Hydrodynamic theory of premixed flames: Effects of stoichiometry, variable transport coefficients and arbitrary reaction orders, Journal of Fluid Mechanics 487 (2003) 179–210.
[14] Y. Rastigejev, M. Matalon, Numerical simulation of flames as gas-dynamic discontinuities, Combustion Theory and Modelling 10 (3) (2006) 459–481.
[15] F. Creta, M. Matalon, Strain rate effects on nonlinear development of hydrodynamically unstable flames, Proceedings of the Combustion Institute 33 (2011) 1087–1094.
[16] F. Creta, M. Matalon, Propagation of wrinkled turbulent flames in the context of hydrodynamic theory, Journal of Fluid Mechanics 680 (2011) 225–264.
[17] C. Altantzis, C. Frouzakis, A. Tomboulides, M. Matalon, K. Boulouchos, Hydrodynamic and thermodiffusive instability effects on the evolution of laminar planar lean premixed hydrogen flames, Journal of Fluid Mechanics 700 (2012) 329–361.
[18] M.L. Frankel, G.I. Sivashinsky, The effect of viscosity on hydrodynamic stability of a plane flame front, Combustion Science and Technology 29 (1982) 207–224.
[19] P. Pelce, P. Clavin, Influence of hydrodynamics and diffusion upon the stability limits of laminar premixed flames, Journal of Fluid Mechanics 124 (1982) 219–237.
[20] Y. Rastigejev, M. Matalon, Nonlinear evolution of hydrodynamically unstable premixed flames, Journal of Fluid Mechanics 554 (2006) 371–392.
[21] F. Creta, N. Fogla, M. Matalon, Turbulent propagation of premixed fames in the presence of Darrieus–Landau instability, Combustion Theory and Modelling 15 (2011) 267–298.
[22] D. Vaynblat, M. Matalon, Stability of pole solutions for planar propagating flames: I. Exact eigenvalues and eigenfunctions, SIAM Journal on Applied Mathematics 60 (2) (2000) 679–702.
[23] D. Vaynblat, M. Matalon, Stability of pole solutions for planar propagating flames: II. properties of eigenvalues/eigenfunctions and implications to stability, SIAM Journal on Applied Mathematics 60 (2) (2000) 703–728.
[24] D. Garrido-Lopez, S. Sarkar, Effects of imperfect premixing coupled with hydrodynamic instability on flame propagation, Proceedings of the Combustion Institute 30 (1) (2005) 621–628.
[25] V. Akkerman, V. Bychkov, L. Eriksson, Numerical study of turbulent flame velocity, Combustion and Flame 151 (3) (2007) 452–471.
[26] N. Peters, H. Wenzel, F.A. Williams, Modification of the turbulent burning velocity by gas expansion, Proceedings of the Combustion Institute 28 (1) (2000) 235–243.
[27] T.C. Treurniet, F.T.M. Nieuwstadt, B.J. Boersma, Direct numerical simulation of homogeneous turbulence in combination with premixed combustion at low Mach number modelled by the G-equation, Journal of Fluid Mechanics 565 (2006) 25–62.
[28] H. Kobayashi, T. Tamura, K. Maruta, T. Niioka, Burning velocity of turbulent premixed flames in a high pressure environment, Proceedings of the Combustion Institute 26 (1996) 389–396.
[29] R.N. Paul, K.N.C. Bray, Study of premixed turbulent combustion including Landau–Darrieus instability effects, Proceedings of the Combustion Institute 26 (1) (1996) 259–266.
[30] H. Kobayashi, Y. Kawabata, K. Maruta, Experimental study on general correlation of turbulent burning velocity at high pressure, Proceedings of the Combustion Institute 27 (1998) 941–948.
[31] Jean-Marie Truffaut, Geoff Searby, Experimental study of the Darrieus–Landau instability on an inverted flame, and measurement of the Markstein number, Combustion Science and Technology 149 (1–6) (1999) 35–52.
[32] D. Bradley, Instabilities and flame speeds in large-scale premixed gaseous explosions, Proceedings of the Royal Society A: Mathematical and Physical Sciences 357 (1999) 3567–3581.
[33] H. Kobayashi, H. Kawakoe, Flame instability effects on the smallest wrinkling scale and burning velocity of high-pressure turbulent premixed flames, Proceedings of the Combustion Institute 28 (2000) 375–382.
[34] D. Bradley, M. Lawes, K. Liu, M.S. Mansour, Measurements and correlations of turbulent burning velocities over wide ranges of fuels and elevated pressures, Proceedings of the Combustion Institute (2012), in press, http://dx.doi.org/10.1016/j.proci.2012.06.060.
[35] A. Soika, F. Dinkelacker, A. Liepertz, Pressure influence on the flame front curvature of turbulent premixed flames: Comparison between experiment and theory, Combustion and Flame 132 (2003) 451–462.
[36] G. Troiani, private communication, Agenzia Nazionale per le Nuove Tecnologie, Rome, Italy, 2012.
[37] N. Fogla, F. Creta, M. Matalon, Influence of the Darrieus–Landau instability on the propagation of planar turbulent flames, Proceedings of the Combustion Institute (2012), in press, http://dx.doi.org/10.1016/j.proci.2012.07.039.
[38] H. Kobayashi, K. Seyama, H. Hagiwara, Y. Ogami, Burning velocity correlation of methane/air turbulent premixed flames at high pressure and high temperature, Proceedings of the Combustion Institute 30 (2005) 827–834.